Clim Dyn
DOI 10.1007/s00382-012-1492-z

Structures and mechanisms of the first-branch northward-propagating intraseasonal oscillation over the tropical Indian Ocean

Kuiping Li · Weidong Yu · Tim Li · V. S. N. Murty · Somkiat Khokiattiwong · T. R. Adi · S. Budi

Received: 11 January 2012 / Accepted: 10 August 2012

Abstract The first-branch northward-propagating intraseasonal oscillation (FNISO) over the tropical Indian Ocean (IO) often triggers the onset of the Asian summer monsoon. In this study we investigate the structures and mechanisms associated with FNISO through the diagnosis of ERA-Interim reanalysis data for the period of 1990–2009. A composite analysis is conducted to reveal the structure and evolution characteristics of the FNISO and associated background circulation changes. It is found that the FNISO convection originates from the southwestern IO and propagates eastward. After reaching the eastern IO, the major convective branch moves northward toward the northern Bay of Bengal (BoB). Two possible mechanisms may contribute to the northward propagation of the FNISO. One is the meridional asymmetry of the background convective instability. A greater background convective instability over the northern BoB may destabilize Rossby waves and cause convection to shift northward. The other is the meridional phase leading of perturbation humidity in the planetary boundary layer (PBL). Maximum PBL moisture appears to the north of the convection center, which promotes a convectively unstable stratification ahead of the convection and leads to the northward propagation of the FNISO. A PBL moisture budget analysis reveals that anomalous zonal advection is a dominant process in contributing to the moisture asymmetry.

Keywords Intraseasonal oscillation · Northward propagation · Monsoon onset

K. Li · W. Yu (✉)
Center for Ocean and Climate Research, First Institute of Oceanography, SOA, Qingdao 266061, China
e-mail: wdyu@fio.org.cn

T. Li
IPRC and Department of Meteorology, University of Hawaii, Honolulu, HI, USA

V. S. N. Murty
National Institute of Oceanography Regional Centre, Visakhapatnam 530017, India

S. Khokiattiwong
Phuket Marine Biology Center, Phuket, Thailand

T. R. Adi · S. Budi
Agency for Marine and Fishery Research and Development, Center for Marine and Coastal Resources Research and Development, Jakarta, Indonesia

1 Introduction

The intraseasonal oscillation (ISO) with a period of 20–70 days is one of the dominant low-frequency signals in the tropical atmosphere (Madden and Julian 1971, 1972). It has been shown that ISO has strong seasonality (e.g., Madden 1986; Wang and Rui 1990; Li and Wang 1994; Salby and Hendon 1994; Zhang and Dong 2004; Li 2010). During boreal winter, maximum ISO activity is confined south of the equator, with predominant eastward or southeastward propagation over the tropical Indian Ocean (IO) (Wang and Rui 1990) and a preferred zonal wavenumber-1 structure (Li and Zhou 2009). During boreal summer, maximum ISO activity shifts to the north of equator, with pronounced northward or northeastward propagation over the IO (Yasunari 1979; Jiang and Li 2005; Wang et al. 2006) and northwestward propagation over the western North Pacific (Murakami 1980; Li and Wang 2005).

The onset of Asian summer monsoon is often triggered by the first-branch northward propagating ISO (FNISO) convection over the Bay of Bengal (BoB, Wang 2006).

Published online: 23 August 2012

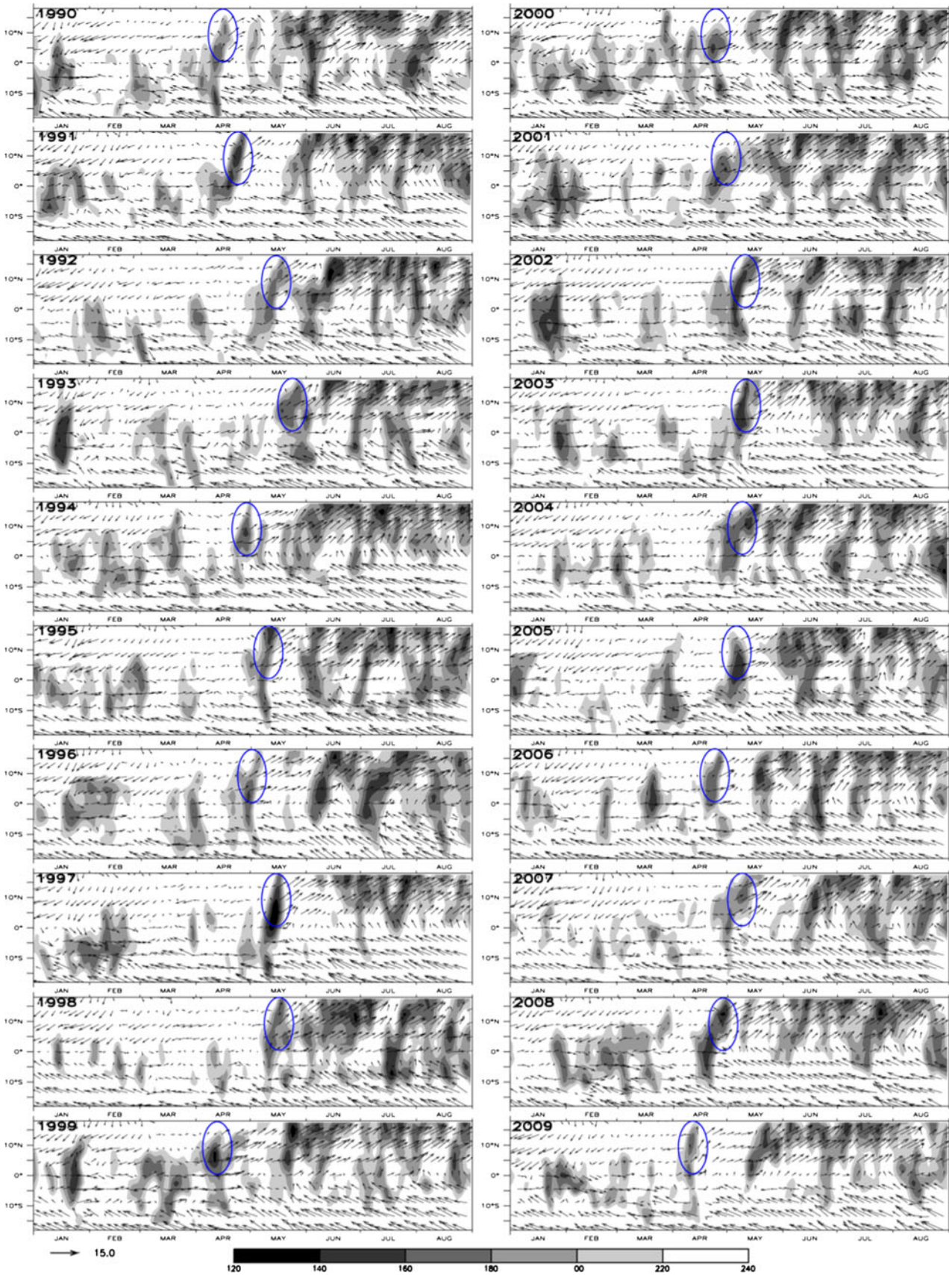
1990
1991
1992
1993
1994
1995
1996
1997
1998
1999
2000
2001
2002
2003
2004
2005
2006
2007
2008
2009
10°N
0°
10°S
JAN FEB MAR APR MAY JUN JUL AUG
15.0
120 140 160 180 00 220 240

◀**Fig. 1** Time-latitude sections of 7-day running mean OLR (*shaded*, W m^{-2}, with values lower than 220 are plotted) and surface wind (*vector*, m s^{-1}) fields along 85°–95°E. The FNISO is defined based on criteria that starting from 1 January, the averaged OLR value at 7.5°–12.5°N first reaches 220 W m^{-2} and the averaged surface westerly in the same region lasts for one week or more

Figure 1 shows the time-latitude section of outgoing longwave radiation (OLR) and surface wind fields over BoB each year from 1990 to 2009. Here the FNISO is highlighted by blue circle in each panel of Fig. 1. As one can see, strong persistent westerlies are found around 5°–15°N each year after the FNISO occurs, indicating the time of the summer monsoon onset. Prior to that, easterlies are pronounced in northern hemisphere, while the ISO convection primarily propagates southward.

Understanding and predicting the FNISO is crucial for prediction of the monsoon onset and for agriculture planning and water management in South Asia. Besides triggering the monsoon, the FNISO also sets up a favorable condition for occurrence of super cyclones in BoB. It was found that five out of total seven super cyclones during 1981–2009 were in phase with the FNISO (Li et al. 2012). For example, Super Cyclone Nargis took place during the FNISO of 2008 and caused devastating flood human loss in Myanmar. Thus a realistic representation and prediction of the FNISO is also critical for tropical cyclone risk assessment.

Previous studies focused on understanding of northward propagation of ISO in boreal summer. The mechanisms responsible for the northward propagation in boreal summer include the meridional asymmetry of moist static energy (Li and Wang 1994; Wu et al. 2006), ocean–atmosphere interaction (Kemball-cook and Wang 2001; Fu et al. 2003), and internal atmospheric dynamics such as vertical shear induced meridional vorticity asymmetry (Jiang et al. 2004; Drbohlav and Wang 2005), meridional vorticity advection (Bellon and Sobel 2008; Dixit and Srinivasan 2011), convective momentum transport (Kang et al. 2010), and meridional humidity asymmetry (Jiang et al. 2004). In all these mechanisms above, the occurrence of the summer mean flow is a necessary condition. However, compared with the summer ISO, a significant difference is that the FNISO takes place in the transitional season when the boreal summer mean flow such as marked easterly shear has not set up yet. Under this transitional background state, what causes the northward propagation of the ISO?

The objective of the current study is to reveal the observed structures and possible mechanisms of the FNISO. The rest of the paper is organized as following. The data and methods are described in Sect. 2. In Sect. 3, we illustrate the evolution patterns of the composite FNISO. The mechanisms for the northward propagation of the FNISO are further presented in Sects. 4 and 5, with an emphasis on the meridional distribution of the background atmospheric convective instability and a meridional phase difference between the FNISO convection and the perturbation humidity. Conclusion and discussion are given in the last section.

2 Data and methods

2.1 Data

The main dataset used in the present study is the daily averaged ERA-Interim archive (Dee et al. 2011) from the European Centre for Medium-Range Weather Forecasts (ECMWF) reanalysis. The data analysis period is from 1990 to 2009, with a horizontal resolution of 1.5° latitude × 1.5° longitude and vertically 23 pressure levels from 1,000 to 200 hPa. Three-dimension variables to be analyzed include zonal and meridional wind components, vertical velocity, divergence, relative vorticity and specific humidity. Observed daily OLR (Liebmann and Smith 1996) from the National Oceanic and Atmospheric Administration (NOAA) is employed as the proxy for convection. To check the reliability of the ERA-Interim reanalysis data, the precipitation field from ERA-Interim is used to compare with the observed OLR pattern. Daily mean surface evaporation from ERA-Interim is also used.

2.2 Methods

One of background variables that possibly affect ISO propagation is atmospheric convective instability. The convective instability parameter is defined as the difference of equivalent potential temperature (θ_e) between the lower and middle troposphere (Zhang et al. 2004; Ding and He 2006):

$$\Delta\theta_e = \theta_e|_{1000-700\,\mathrm{hPa}} - \theta_e|_{600-300\,\mathrm{hPa}}$$

A positive value of $\Delta\theta_e$ implies that the atmosphere is potentially unstable. By examining the $\Delta\theta_e$ pattern, one may infer where the atmosphere favors the development of convection.

For all dynamic and thermodynamic variables, the ISO signal is isolated by a 20–70-day band-pass filter and then symbolized by a prime. To illustrate the role of the background state in causing the northward propagation of ISO convection, the low-frequency component with period longer than 90-day is extracted by a low-pass filter and then symbolized by an over bar.

3 Composite evolution features of the FNISO

First we illustrate the composite evolution patterns of the FNISO averaged along 80°–100°E for the period of

1990–2009. The composite was made based on the 20 FNISO cases, with a reference date on which the FNISO convection (represented by minimum OLR center) arrives at 10°N. Figure 2a shows the composite evolution patterns of OLR, rainfall and surface wind fields. Before the first branch of the northward propagation, convection is mainly confined to south of the equator, and northeasterlies are pronounced in northern hemisphere. Sustained southwesterly winds are set up in northern hemisphere, and successive northward propagating events are observed after the onset of the FNISO. Along the forehead of the FNISO, the easterly vertical shear extends northward to 20°N from about 5°N (Fig. 2b). The northerly vertical shear is triggered by the FNISO convection center, reaching more than 10°N starting from the equator.

In both Figs. 1 and 2, total fields are used to illustrate the climatologic features. To examine the initiation and detailed evolution characteristics of the ISO, we apply a 20–70-day band-pass filter to the OLR, rainfall and surface wind fields. Figure 3 shows the time sequence (with a 3-day interval) of the composite FNISO evolution patterns. Same as Fig. 2, day 0 is referred to as when maximum FNISO convection arrives at 10°N, 80°–100°E. Note that the FNISO convection initiates at the southwestern IO at day −15. Then, it quickly moves eastward while gradually shifts to north. At day −6, the major convection arrives at the eastern equatorial IO. After that, the major convective branch moves northward over the BoB. Meanwhile, a weak branch continues to eastward propagate and gets strengthened after passing across the marine continent.

To check the reliability of the reanalysis data, the ERA-Interim precipitation field is also plotted in Figs. 2a and 3, in comparison with the observed OLR patterns. As seen from these figures, both have a great similarity in the spatial and temporal evolution characteristics. This verifies the reliability of the reanalysis data.

4 Role of the asymmetry of background convective instability

The composite evolution patterns in Fig. 3 illustrate that FNISO convection starts to propagate northward after passing the central equatorial IO. A natural question is what the role of background mean state is in triggering the northward propagation. To address the question, we

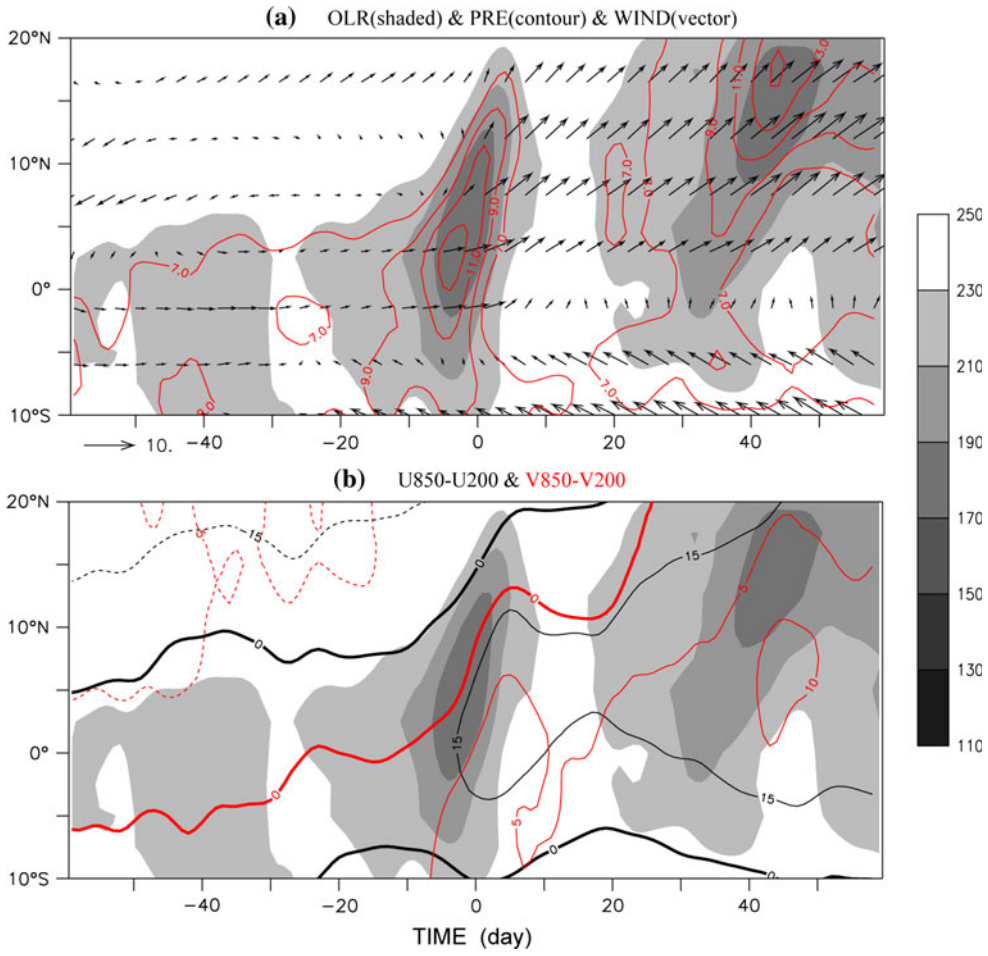

Fig. 2 Composite time-latitude sections along 80°–100°E: **a** OLR (*shaded*, W m^{-2}), surface wind (*vector*, m s^{-1}) and rainfall (*contour*, mm day^{-1}) fields; **b** vertical difference between 850 and 200 hPa in zonal wind (*black contour*, m s^{-1}) and meridional wind (*red contour*, m s^{-1}) overlaid on OLR (*shaded*, W m^{-2}). The vertical axis is latitude, and the horizontal axis is the relative time, with day 0 representing the date when maximum FNISO convection arrives at 10°N

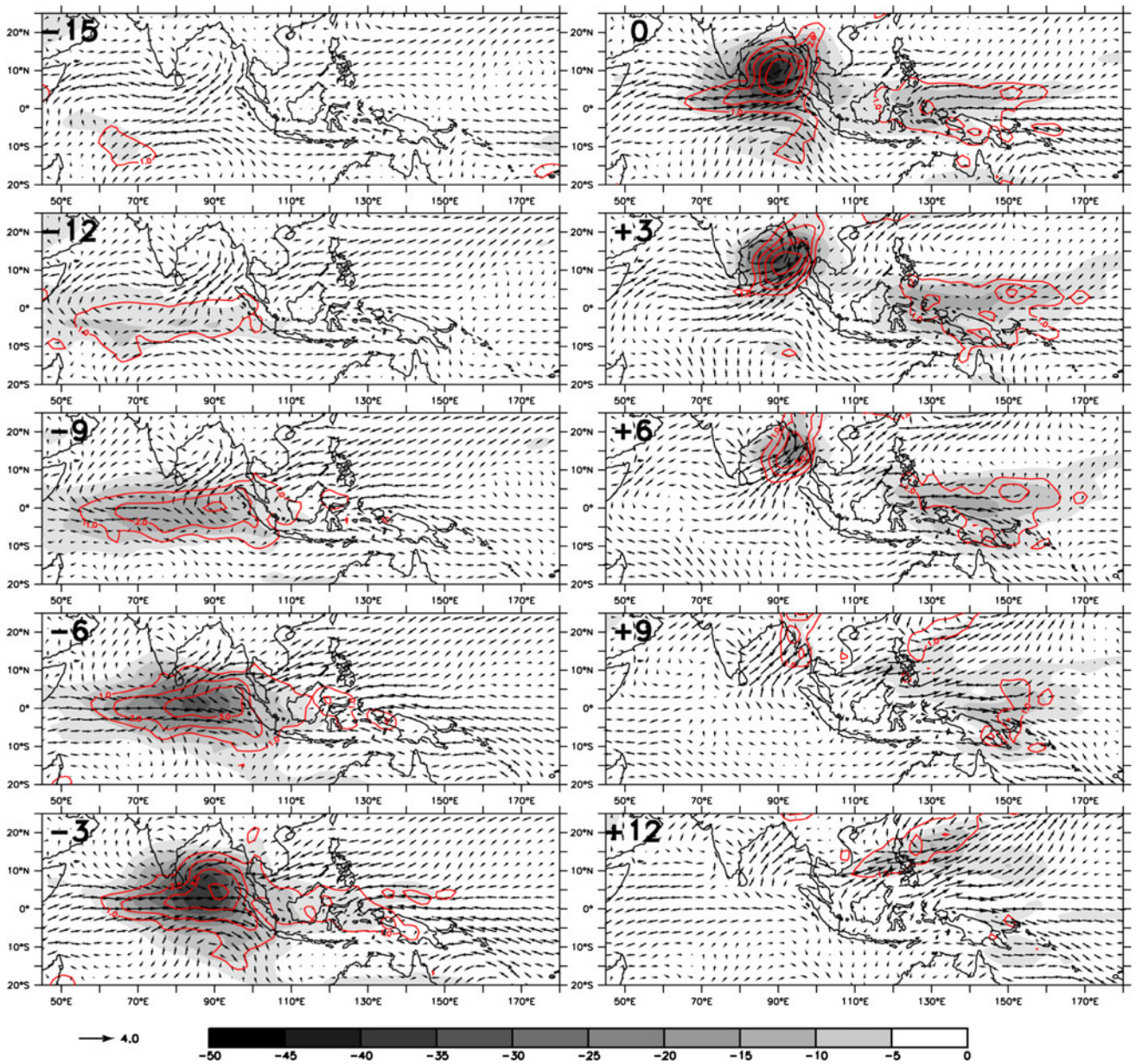

Fig. 3 Composite evolution patterns of the 20–70-day filtered OLR (*shaded*, W m^{-2}), rainfall (*contour*, mm day^{-1}) and surface wind (*vector*, m s^{-1}) fields associated with the FNISO. Day 0 is a reference day when maximum FNISO convection arrives at 10°N in the eastern IO

examine the distribution of background convective instability parameter ($\overline{\Delta\theta_e}$) averaged between day −20 and day 0 (Fig. 4a). It is interesting to note that a marked equatorial asymmetry appears in the eastern IO in the $\overline{\Delta\theta_e}$ field. Maximum (minimum) background convective instability appears north of 10°N (south of 10°S). A reversed meridional asymmetry of background convective instability appears in the western IO. The east–west contrast in the background convective instability pattern is consistent with the east–west difference in ISO behavior (Hsu and Li 2012), that is, in the western IO ISO activity is most confined to the south of the equator, whereas in the eastern IO major branch of ISO convection moves northward (Fig. 3).

The result above suggests that the low-frequency background state may control the ISO propagation characteristics. Dynamically how does the background convective instability field affect ISO propagation? We argue that it is through the modulation of relative strength of equatorial Kelvin and Rossby waves. The ISO may be regarded as a Kelvin–Rossby wave couplet (Wang and Li 1994). While precipitation signals associated with the Kelvin waves are primarily confined in the equatorial zone (between 10°S and 10°N), the Rossby wave has a maximum vorticity

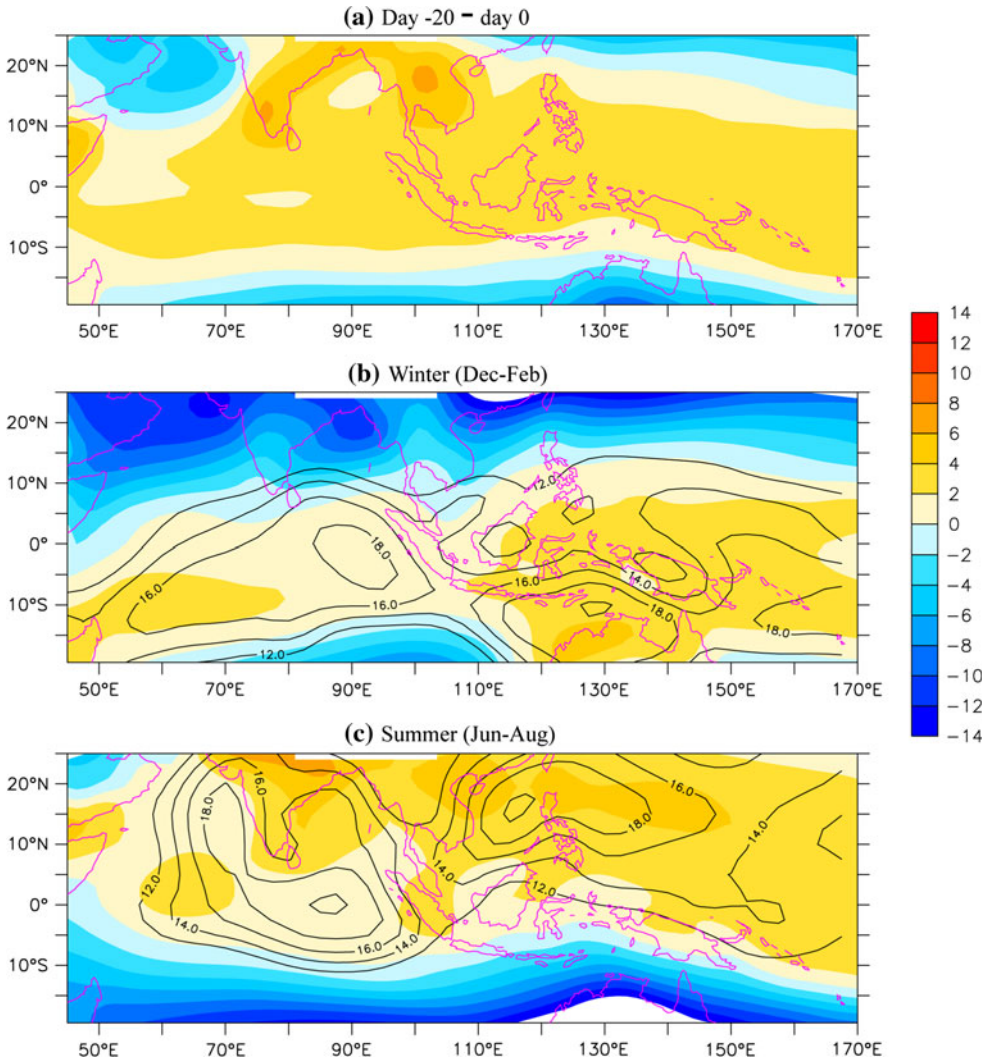

Fig. 4 Distribution of the background (low-frequency component with period longer than 90-day) convective instability ($\overline{\Delta\theta_e}$, *shaded*, K) field during **a** day −20 to day 0, **b** boreal winter, and **c** boreal summer. The seasonal mean ISO activity is indicated by overlaid contours at (**b**) and (**c**), represented by the standard deviation of 20–70-day filtered OLR (W m^{-2})

center away from the equator. During northern winter, maximum mean convection or mean convective instability is confined in the equatorial zone (within 10°S and 10°N); as a result, the Kelvin wave is unstable and precipitation signals associated with the Kelvin–Rossby wave couplet are confined in the equatorial zone and propagate eastward. During northern summer, maximum mean convection or mean convective instability is located along the monsoon trough (15°N); as a result, the Kelvin wave is stabilized while the Rossby wave is destabilized (Li and Wang 1994). This leads to a shift of maximum rainfall from the equator to the Rossby gyre center north of the equator (Zhu et al. 2010). Thus the meridional distribution of the background convective instability plays an important role in determining the ISO propagation behavior.

To clearly illustrate the relationship between the mean state and ISO characteristics, we plot both the background convective instability parameter ($\overline{\Delta\theta_e}$) and ISO activity (represented by standard deviation of 20–70-day band-pass filtered OLR) in Fig. 4b, c. It is evident that the ISO characteristics are closely related to the distribution of the background convective instability. During both boreal summer and winter seasons, strong ISO activity is mainly confined to the regions with positive value of $\overline{\Delta\theta_e}$. This implies that the mean state exerts a large-scale control on ISO development. A stronger meridional asymmetry (relative to the equator) of $\overline{\Delta\theta_e}$ is observed in boreal summer than winter. This is consistent with the fact that the ISO has a pronounced northward (eastward) propagation in boreal summer (winter).

The meridional asymmetry of the background convective instability in the eastern IO during the transitional period (day −20 to day 0) resembles, to a large extent, the boreal summer condition. This is why the convection associated with the FNISO shifts northward after passing the central IO.

The observational evidence above suggests that the setup of an asymmetric background convective instability

field is crucial in causing the northward propagation of the FNISO convection over the eastern IO. Next we address how the asymmetric background state in the eastern IO is established. Figure 5a illustrates the temporal evolution of the background convective instability field averaged along 80°–100°E. Note that $\overline{\Delta\theta_e}$ is negative north of 5°N prior to day −30. During that time ISO convection is mainly confined in the equatorial region. After that, $\overline{\Delta\theta_e}$ gradually increases in northern hemisphere, and at about day −20 the averaged value in northern hemisphere is greater than that in southern hemisphere. This basic state change sets up the onset of the FNISO.

To quantitatively measure the change of the convective instability, we define a convective instability parameter as the average of $\overline{\Delta\theta_e}$ from 5° to 25°N along 80°–100°E. The black line in Fig. 5b illustrates the time evolution of this parameter. Starting from a negative value, the parameter exhibits a continuously increasing trend, crossing the zero line at about day −40.

As the change of equivalent potential temperature is determined by the change of specific humidity (q) and air temperature (T), what are their relative roles in causing the increase of $\overline{\Delta\theta_e}$ over the northern BoB? To address this question, we re-calculate $\overline{\Delta\theta_e}$ using either $(\bar{T}, \bar{q}_0)$ or $(\bar{T}_0, \bar{q})$, with $(\bar{T}_0, \bar{q}_0)$ being the value at day −60. The former reflects a partial contribution from the variation of $\bar{T}$ (hereafter referred to as $T-$induced $\overline{\Delta\theta_e}$), whereas the latter represents a partial contribution from the variation of $\bar{q}$ (hereafter referred to as $q-$induced $\overline{\Delta\theta_e}$). Our calculation shows that the increase of $\overline{\Delta\theta_e}$ is primarily attributed to the contribution of the specific humidity field (green line in Fig. 5b).

Considering the period from day −60 to day 0, we next examine to what extent the $\overline{\Delta\theta_e}$ increase is contributed by the change of specific humidity at the low level (1,000–700 hPa) and upper level (600–300 hPa). Here a symbol "δ" is introduced to represent the time difference between day 0 and day −60, that is, $\delta\left(\overline{\Delta\theta_e}\right) = \overline{\Delta\theta_e}\big|_{0\,\mathrm{day}} - \overline{\Delta\theta_e}\big|_{-60\,\mathrm{day}}$. Figure 6 shows the value of $\delta\left(\overline{\Delta\theta_e}\right)$ and relative contributions of the low-level and upper-level $\delta\overline{\theta_e}$. It turns out that $\overline{\Delta\theta_e}$ increases from day −60 to day 0 by 6.4 K, and this increase is mainly contributed by low-level

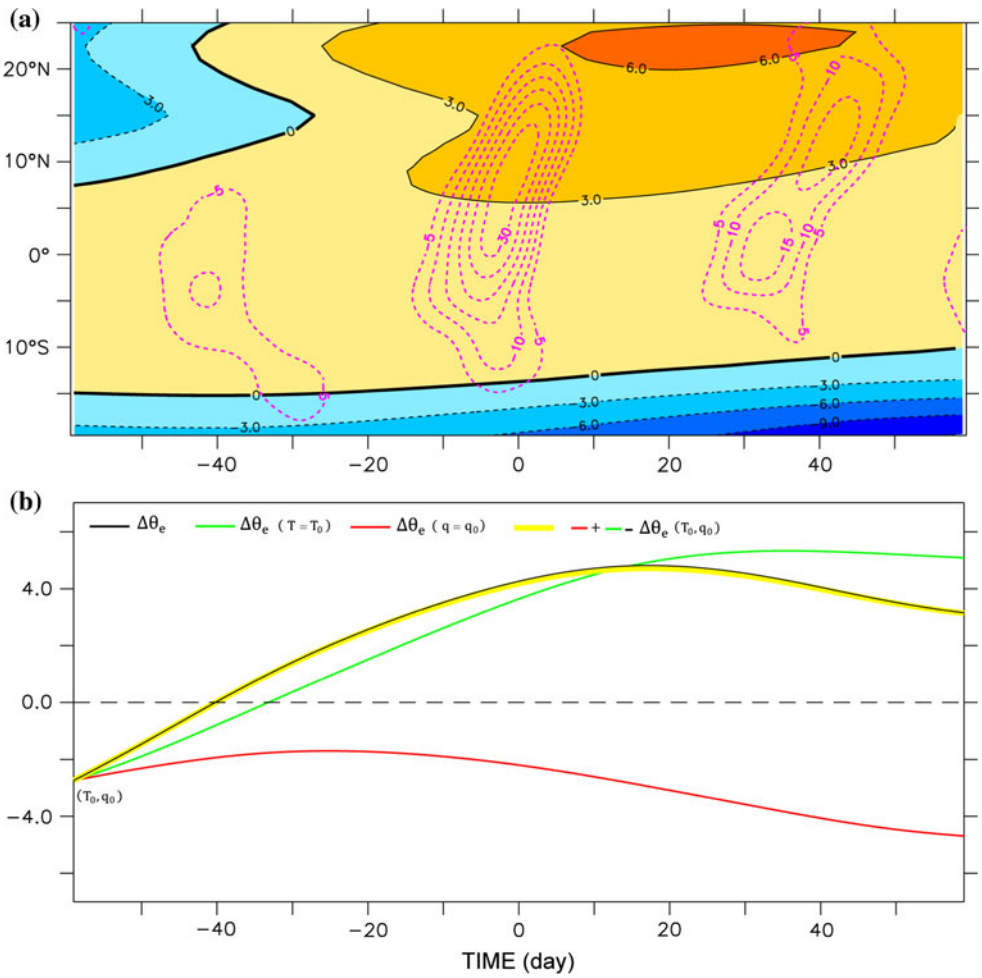

Fig. 5 **a** Time-latitude section of the background convective instability field (*shaded*, K) and the OLR perturbation associated with FNISO (*contour*, Wm^{-2}) along 80°–100°E; **b** time evolution of $\overline{\Delta\theta_e}$ (*black line*, K) and the partial contributions of $\overline{\Delta\theta_e}$ due to the temperature (*red*) and moisture (*green*) changes averaged over the region [80°–100°E, 5°–25°N]. The sum of the two partial contributions is plotted by a *yellow curve*. The horizontal axis is the time (unit: day) relative to the same reference day 0 shown in Fig. 3

$\delta\overline{\theta_e}$ (9.6 K) while the upper-level $\delta\overline{\theta_e}$ has a negative contribution of −3.2 K. Thus it is concluded that the enhanced background convective instability in the northern hemisphere is primarily attributed to the increase of the low-level specific humidity over the eastern IO.

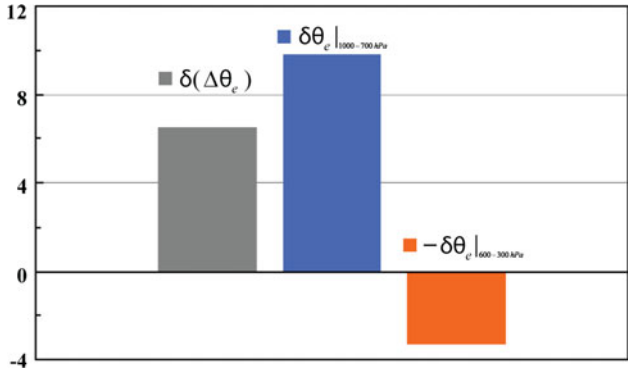

Fig. 6 Difference (day 0 minus day −60) of the background convective instability parameter (defined as an averaged value of $\overline{\Delta\theta_e}$ over 80°–100°E and 5°–25°N, *gray bar*, K) and relative contributions from the low level (averaged over 1,000–700 hPa, *blue bar*, K) and the upper level (averaged over 600–300 hPa, *orange bar*, K)

A moisture budget was further conducted to examine specific processes that cause the increase of the low-level specific humidity north of the equator. Following Yanai et al. (1973), a moisture tendency equation may be written as:

$$\frac{\partial\bar{q}}{\partial t} = -\overline{(\mathbf{V}\cdot\nabla q)} - \overline{\left(w\cdot\frac{\partial q}{\partial p}\right)} - \overline{(Q_2/L)} \tag{4.1}$$

where $\mathbf{V}$ is the horizontal velocity, w is the p-vertical velocity, Q_2 is apparent moisture sink, and L is latent heat constant. In the equation above, $-\overline{(V\cdot\nabla q)}$ denotes horizontal moisture advection, $-\overline{\left(w\cdot\frac{\partial q}{\partial p}\right)}$ indicates vertical moisture advection, and $-\overline{(Q_2/L)}$ represents the moisture source or sink (primarily determined by surface evaporation and atmospheric condensation). The diagnosis of the low-level $\bar{q}$ was done from day −60 to day 0.

As seen from Fig. 7a, a positive $\bar{q}$ tendency covers the northern BoB and surrounding region. The horizontal advection term has a large positive value over the northern IO while a negative value over the surrounding land regions (Fig. 7b). The maximum positive contribution from the vertical advection is mostly located at the vicinity of

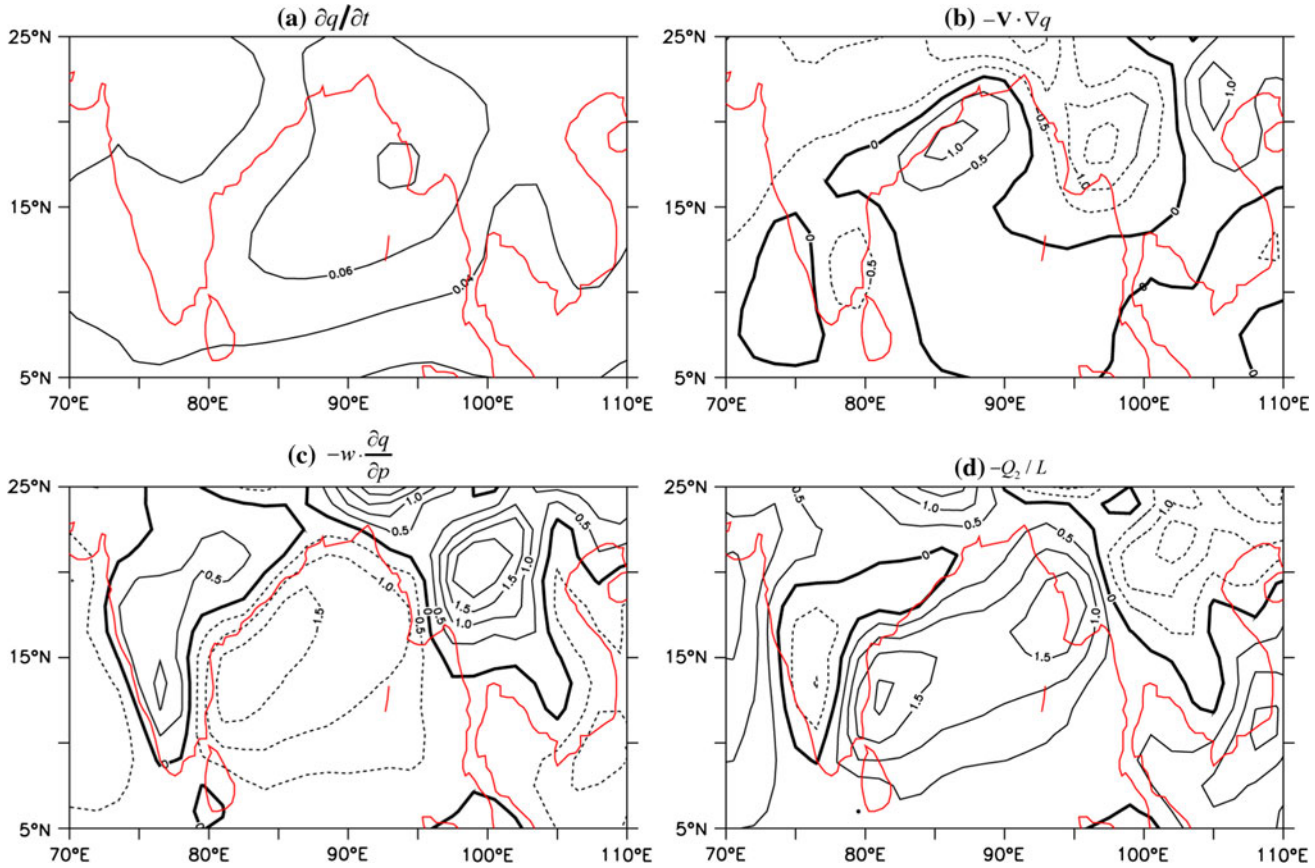

Fig. 7 Spatial distributions of the vertically averaged (1,000–700 hPa) **a** $\bar{q}$ tendency, **b** horizontal moisture advection term, **c** vertical moisture advection term, and **d** moisture sink term (unit: g day^{-1}) in Eq. 4.1 during the period of day −60 to day 0

land, whereas the negative contribution appears over the BoB (Fig. 7c). The ocean surface evaporation obviously plays a role in moistening the low-level atmosphere over the BoB (Fig. 7d).

To understand the patterns of the above diagnostic terms, we examine the low-level wind, specific humidity and air temperature distributions averaged between day −60 and day 0 (Fig. 8). Compared with pronounced trade winds over the southern hemisphere, circulation over the northern hemisphere looks more complicated (Fig. 8a). Note that near-surface air temperature is much warmer over the land of the Indian subcontinent and the Indochina peninsula, while it is relatively cool over the northern BoB (Fig. 8b). As a result, cyclonic flows appear over the warmer land regions whereas anti-cyclonic circulation appears over the cooler ocean. Moist transport along the east coast of Indian subcontinent primarily contributes to the positive horizontal advection over the northern BoB. The low-level divergence associated with the anti-cyclonic circulation over the northern BoB leads to subsidence and thus negative vertical moisture advection in situ. Because of the subsidence, less rainfall is resulted over the region. Therefore, the northern BoB is an apparent moisture source as a result of evaporation exceeding precipitation (Fig. 8c).

To sum up, the evidence presented above suggests that the meridional asymmetry of the background convective instability is responsible for the northward propagation of the FNISO over the eastern IO. The setup of the background convective instability is primarily attributed to the increase of low-level specific humidity in the northern IO and surrounding land regions. A moisture budget analysis reveals that the positive moisture tendency is ultimately driven by the land-sea thermal contrast over the region.

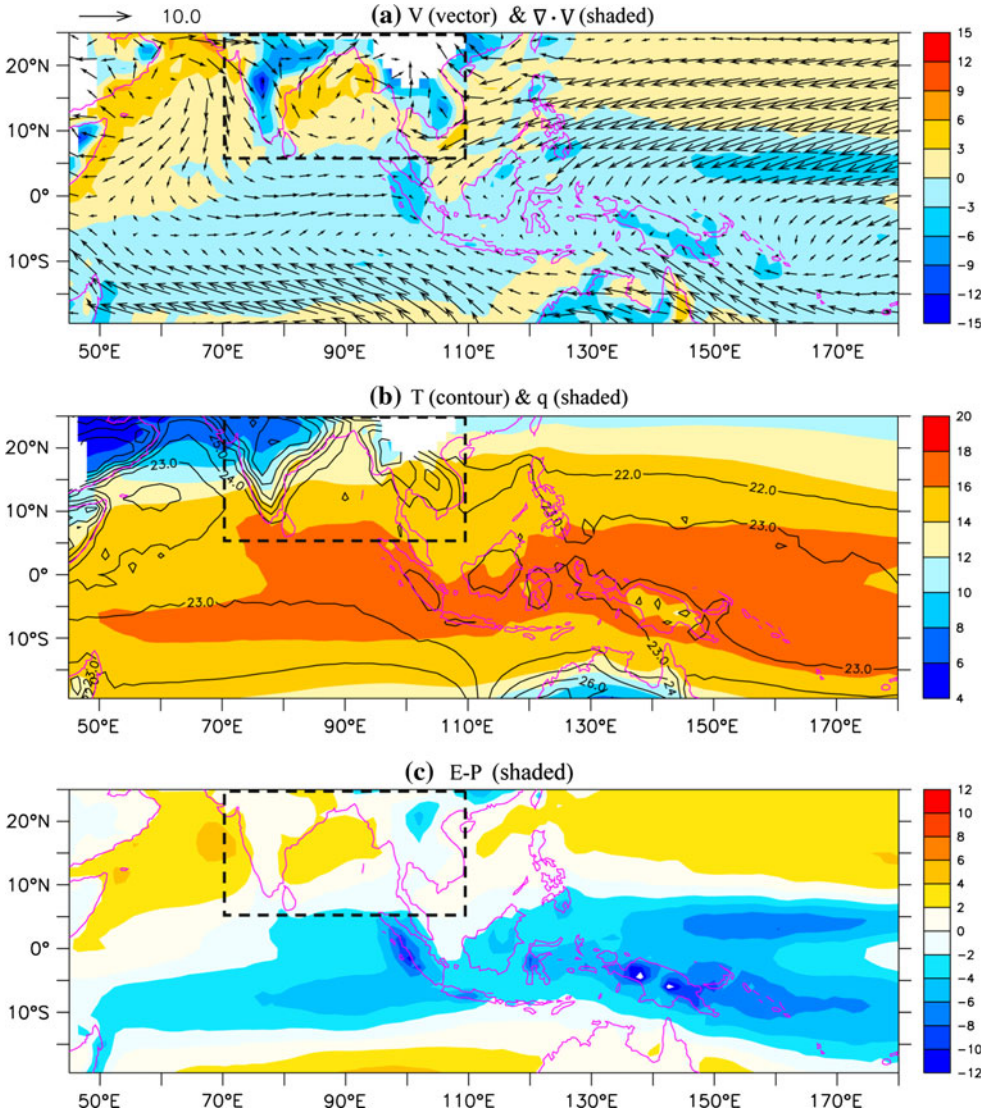

Fig. 8 Distribution of **a** the background 950-hPa wind (*vector*, m s^{-1}) and divergence (*shaded*, 10^{-6} s^{-1}) fields, **b** 950-hPa air temperature (*contour*, °C) and specific humidity (*shaded*, g kg^{-1}) fields, and **c** evaporation minus precipitation (*shaded*, g day^{-1}) field averaged from day −60 to day 0

5 Effect of meridional asymmetry of perturbation humidity

In the previous section, we focused on the role of the background state. In this section we shift our attention to the structures of the ISO itself. It has been shown that the northward propagation of ISO in boreal summer is associated with a boundary layer convergence that leads the convection (Lawrence and Webster 2002; Jiang et al. 2004; Goswami 2005). The cause of the phase leading of the convergence was attributed to a leading of relative vorticity associated with the summer mean vertical shear (Jiang et al. 2004) or vorticity advection by mean meridional baroclinic flow (Bellon and Sobel 2008). Now, in the absence of the summer mean flow, could these characteristics be found in the FNISO?

Following Jiang et al. (2004), a composite analysis was conducted to reveal the meridional-vertical structures of the FNISO. The composite was made in relevance to the ISO convection center at 7.5°, 10°, 12.5°, and 15°N along 80°–100°E. Figure 9 shows the meridional–vertical section of the composite FNISO derived from the ERA-Interim reanalysis. Each field was interpolated from the original 1.5° interval to 0.5° in the meridional direction by a cubic-spline method, and was applied a 20–70-day band-pass filter prior to the composite analysis.

Compared with the boreal summer ISO structures (see Fig. 8 in Jiang et al. 2004), a significant difference is that the positive vorticity (and low-level convergence) field does not lead the convection center (Fig. 9a, b). This is because the northward propagation happens during the transitional season when the background flow including the marked vertical shear has not set up yet (Fig. 2b). The meridional asymmetry of the low-level specific humidity, on the other hand, is clearly seen (Fig. 9c). For example, maximum perturbation specific humidity in PBL (1,000–850 hPa) appears at about 400 km north of the convection center. Such a PBL moistening would precondition the convective instability to the north of the ISO convection (Hsu and Li 2012), leading to the northward propagation of the FNISO.

A perturbation moisture budget analysis was performed to reveal mechanisms responsible for the moisture increase ahead of the convection. Similar to (4.1), a tendency equation for q' may be written as:

$$\frac{\partial q'}{\partial t} = -(\mathbf{V}\cdot\nabla q)' - \left(w\cdot\frac{\partial q}{\partial p}\right)' - (Q_2/L)' \tag{5.1}$$

The meridional-vertical sections of each perturbation moisture tendency terms were shown in Fig. 10. A striking meridional asymmetry is clearly presented in the vertical cross section of the q' tendency, with a maximum positive center appearing 400–800 km north of the ISO convection center (Fig. 10a). The vertical advection term and the moisture sink term are largely offset, as seen from Fig. 10c, d, and both the terms are approximately symmetric to the ISO convection center and thus do not play an important role in causing the PBL moisture asymmetry. To the first order, the meridional asymmetry of the PBL q' tendency is determined by the horizontal advection term, which shows a large positive contribution at 400–800 km north of the convection center and a negative contribution at and south of the convection center (Fig. 10b).

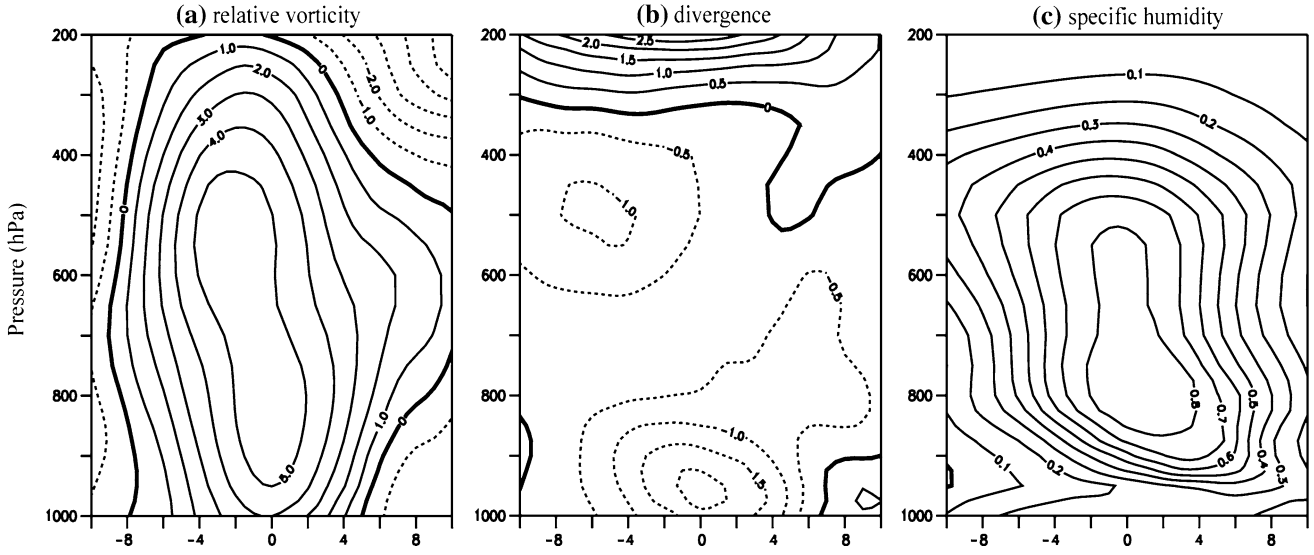

Fig. 9 Meridional–vertical sections of the composite FNISO fields along the 80°–100°E: **a** relative vorticity (10^{-6} s^{-1}), **b** divergence (10^{-6} s^{-1}), and **c** specific humidity (g kg^{-1}). Horizontal axis is the meridional distance (°lat) relative to the ISO convection center, with positive (negative) value meaning northward (southward). The vertical axis is the pressure (hPa)

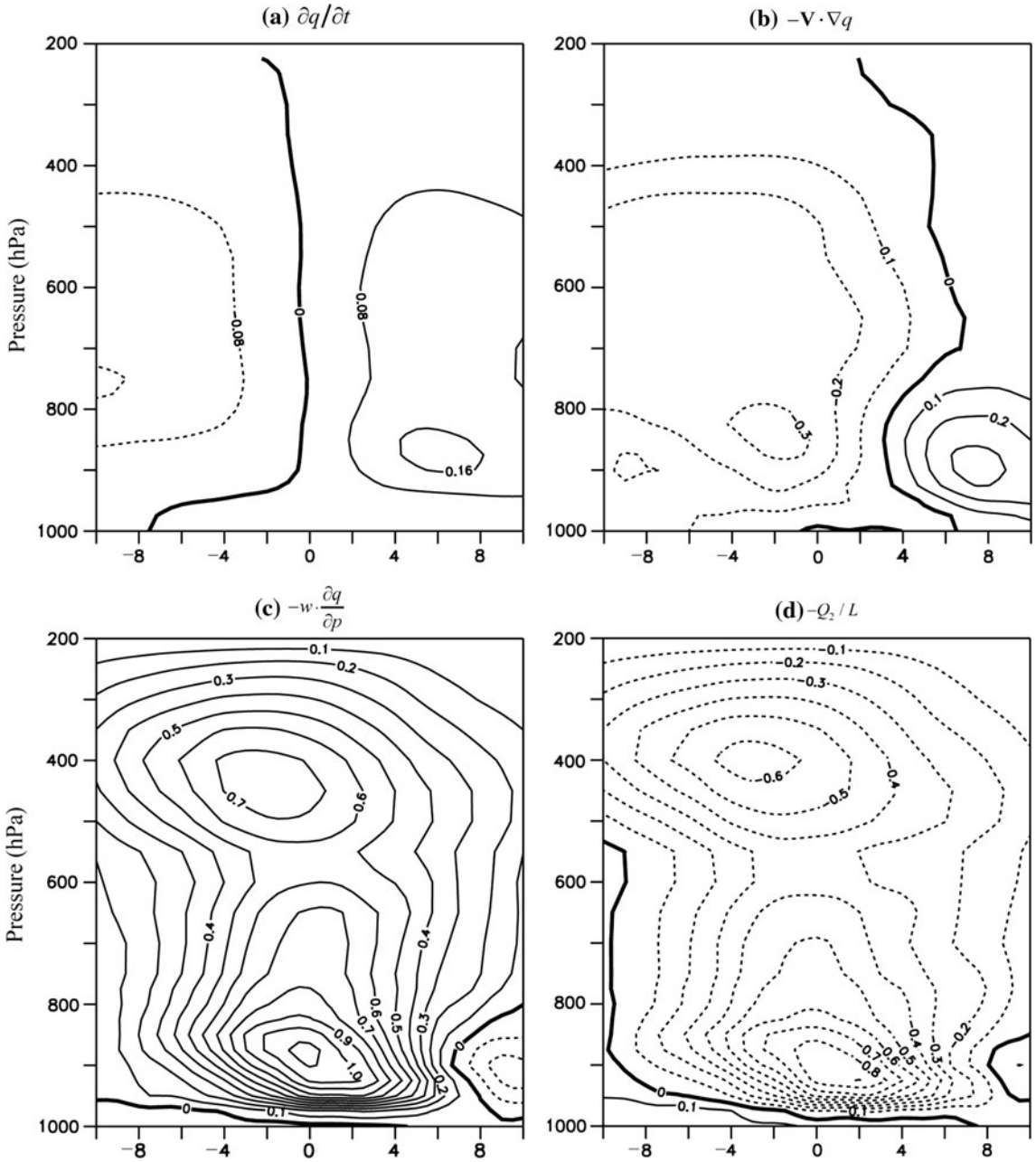

Fig. 10 As in Fig. 9, but for the diagnostic terms in Eq. 5.1: **a** q' tendency, **b** horizontal moisture advection term, **c** vertical moisture advection term, and **d** moisture sink term (unit: g day^{-1})

To better show the meridional distribution, PBL-integrated q' tendency terms are shown in Fig. 11a. It is noted that the combined vertical advection and moisture sink term shows a negative tendency 500 km and beyond to the north of the convection center. Thus the two terms do not contribute to the PBL moistening at 400–800 km. The moistening in the region is primarily attributed to the horizontal advection term.

In interpreting the northward shift of PBL humidity, Jiang et al. (2004) emphasized anomalous moisture advection by the mean meridional wind ($-\bar{v}\cdot q'_y$) and anomalous moisture advection by the perturbation meridional wind in the presence of the mean moisture gradient ($-\bar{v}\cdot q'_y$). It was shown that the former is dominant over the BoB during boreal summer (Chou and Hsueh 2010). Dose the same process operate during the FNISO period?

The horizontal advection term may be separated into both the zonal and meridional components. Figure 11b shows the contributions from four major terms. It is found that in the key moistening region (i.e., 400–800 km north

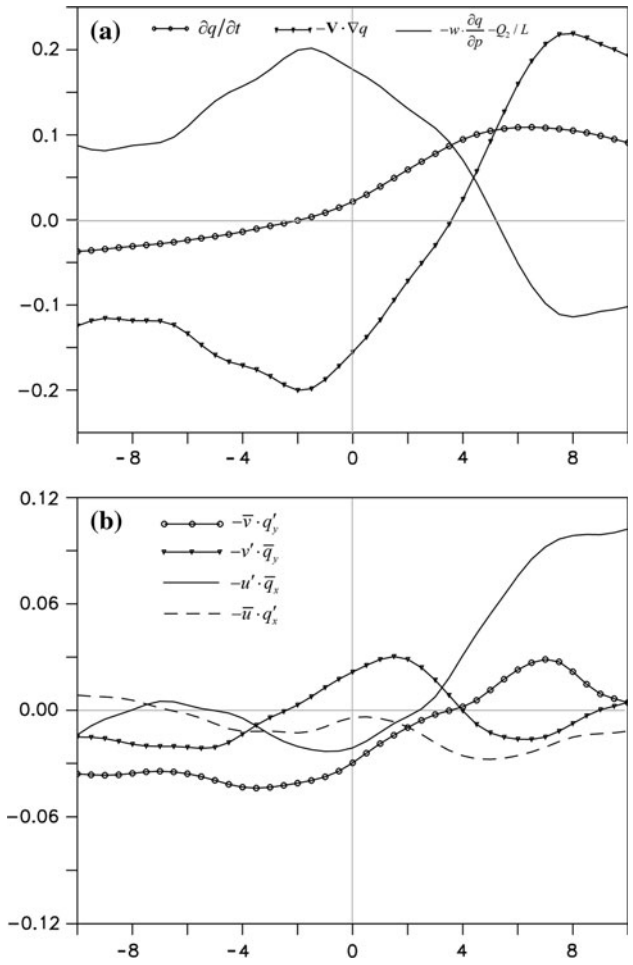

Fig. 11 Meridional distributions of the PBL-integrated (1,000–850 hPa) **a** diagnostic terms in Eq. 5.1, and **b** decomposed horizontal advection term (unit: g day^{-1}). The horizontal axis is the relative distance same as in Fig. 9

of the convection center) $-\bar{v}\cdot q'_y$ has a positive contribution while $-\bar{v}\cdot q'_y$ has a negative contribution, and the two terms are largely offset with each other. Compared with the meridional advection, advection by the perturbation zonal wind due to mean moisture gradient ($-u'\cdot\bar{q}_x$) has a much stronger effect for the FNISO.

The difference of the anomalous zonal and meridional advection effects may be better understood by comparing the values of (u', $\bar{q}_x$) and (v', $\bar{q}_y$) as illustrated in Fig. 12. While the zonal and meridional gradients are comparable, the PBL zonal wind anomaly is about 3–5 times as large as the meridional wind anomaly, particularly in the region ahead of the convection. Thus, our diagnosis reveals the important role of $-u'\cdot\bar{q}_x$ in the PBL moisture asymmetry during the FNISO. Whether or not this zonal advection effect is important for northward-propagating ISOs during boreal summer is an interesting question and requires a further observational analysis.

To sum up, unlike a typical boreal summer ISO, there is no phase leading in relative vorticity (as well as low-level convergence) field relative to the FNISO convection in the absence of the summer mean flow. The meridional asymmetry of the PBL moisture responsible for the northward propagation is primarily caused by the meridional contrast of anomalous zonal advection.

6 Conclusion and discussion

In this paper, the structures and mechanisms of the first-branch northward-propagating ISO (FNISO) were investigated through the diagnosis of the ERA-Interim reanalysis and observed OLR data for the period of 1990–2009. A composite analysis shows that the FNISO convection originates from the southwestern IO. During the course of eastward propagation, the convection center gradually shifts to the north. The major convective branch moves northward over the eastern IO.

Different from the summertime ISO, the northward propagation of the FNISO takes place in the absence of the summer mean flow. This unique feature motivates us further to investigate physical mechanisms responsible for the northward propagation of the FNISO. Two possible mechanisms are proposed based on the observational analysis.

The first mechanism is attributed to the meridional asymmetry of the background atmospheric convective instability. The composite result shows that a notable asymmetry of background convective instability between northern and southern hemisphere is established over the eastern IO prior to the FNISO. Such a background condition favors the destabilization of Rossby waves and thus the northward shift of the FNISO convection. The increase of convective instability over the BoB is primarily attributed to the increase of low-level specific humidity. A moisture diagnosis analysis further reveals that the increase of the moisture is caused by circulation patterns associated with the land-sea thermal contrast during the period.

The second mechanism is due to the distinct meridional phase structures of the FNISO. The observational analysis reveals a meridional phase difference between the FNISO convection and the low-level perturbation humidity. That is, the maximum PBL moisture is located at the north of the ISO convection center. Such a PBL moistening may precondition the atmospheric convective instability to the north of the ISO convection center, leading to the onset of new convection and thus the northward propagation. A PBL moisture budget diagnosis shows that the increase of the perturbation humidity is largely due to the zonal moisture advection.

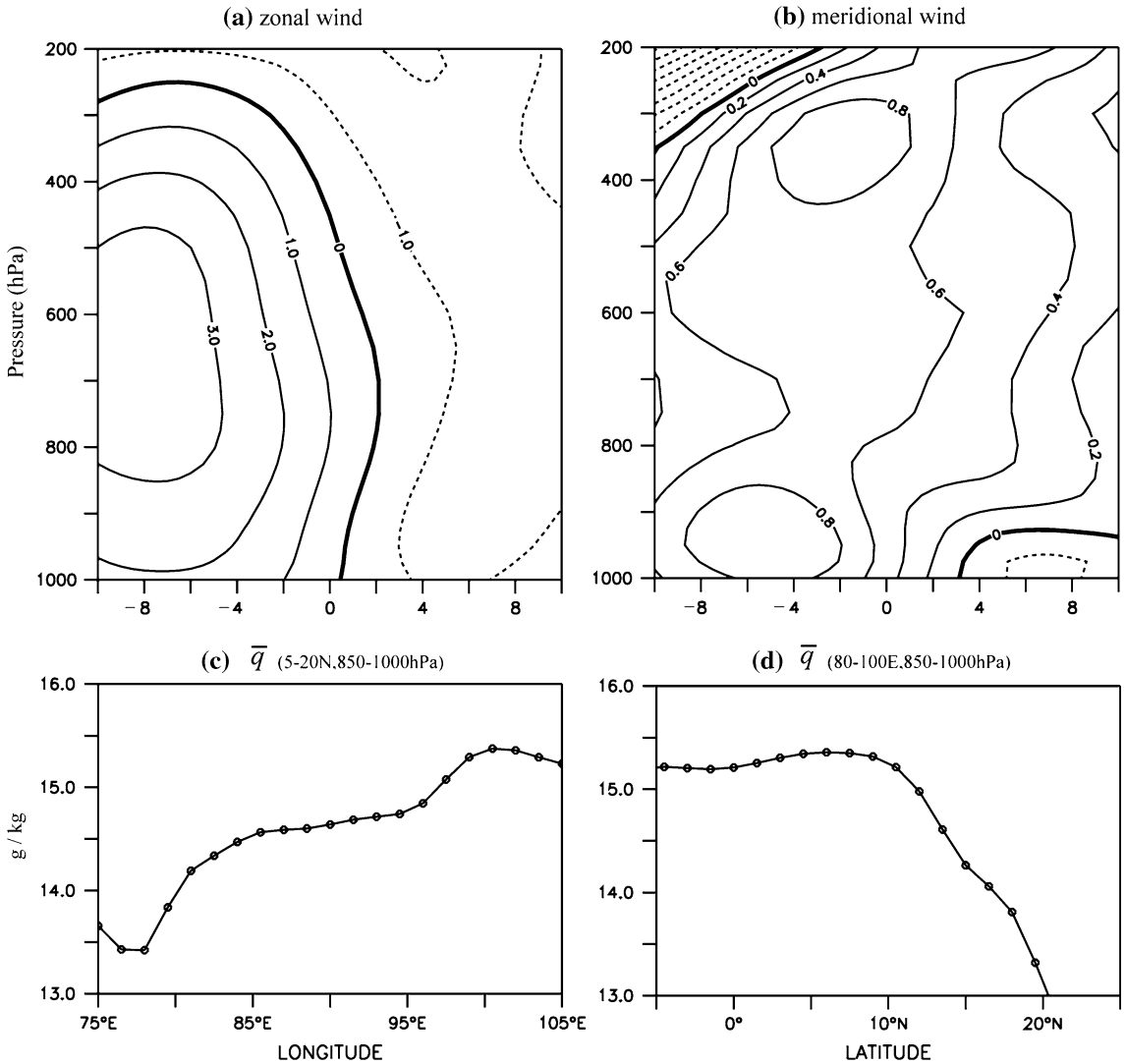

Fig. 12 (*top panel*) Meridional–vertical sections of **a** perturbation zonal wind and **b** meridional wind (m s^{-1}) associated with the FNISO along 80°–100°E. (*bottom panel*) The background specific humidity profiles along **c** 5°–20°N and **d** 80°–100E° averaged in the boundary layer (1,000–850 hPa, g kg^{-1}) from day −10 to day +10

The composite FNISO structures show that unlike a typical summertime ISO event (e.g., Jiang et al. 2004), there is no obvious phase leading in the perturbation vorticity and low-level convergence fields. This is because in the transitional season the summer mean flow has not set up yet. This points out the uniqueness of the FNISO in comparison with general northward-propagating boreal summer ISO events.

In this study two possible mechanisms for the FNISO are proposed based on the observational analysis. One issue related to the two mechanisms is whether the two mechanisms work together or independently. It is worth noting that the composite ISO meridional structure in Fig. 9 was derived based on the convection at 7.5°–15°N. Thus the moisture asymmetry mechanism can only apply to off-equatorial region. On the other hand, the asymmetric background convective instability field is argued to be responsible for the destabilization of Rossby waves and thus the initial shift of ISO convection from the equator to the Rossby gyre center (typically located around 5°–10°N). Once the heating is shifted to the Rossby gyre center, the system can further move northward through the meridional moisture asymmetry mechanism. The argument above suggests that both mechanisms need work together to cause the northward propagation of the FNISO.

In this study we hypothesize that the background mean state determines the instability of equatorial Kelvin and Rossby waves. This requires further theoretical analysis and/or modeling validation. Further studies are also needed to understand the role of the other environmental conditions and multi-scale interactions in causing the FNISO.

Acknowledgments This work was supported by Chinese MoST grants 2009DFA21000, 2010CB950303, NSFC grant 41005032, SOA grant 2011246 and FIO grant 2008T02. This research is part of the Southeast Asian Global Ocean Observation System (SEAGOOS) pilot project entitled Monsoon Onset Monitoring and its Social and Ecosystem Impacts (MOMSEI) under the Sub-Commission for Western Pacific of the Intergovernmental Oceanographic Commission (IOC-WESTPAC). Tim Li was supported by NSF AGS-1106536 and by the International Pacific Research Center that is sponsored by the Japan Agency for Marine-Earth Science and Technology (JAMSTEC), NASA (NNX07AG53G) and NOAA (NA17RJ1230). This research is also part of the collaboration program between the National Institute of Oceanography/Council of Scientific and Industrial Research (NIO/CSIR) and the National Science Foundation of China (NSFC). This is SOEST contribution number 8725, IPRC contribution number 905 and NIO contribution number 5220.

References

Bellon G, Sobel AH (2008) Instability of the axisymmetric monsoon flow and intraseasonal oscillation. J Geophys Res 113:D07108. doi:10.1029/2007JD009291

Chou C, Hsueh YC (2010) Mechanisms of northward-propagating intraseasonal oscillation—a comparison between the Indian Ocean and the Western North Pacific. J Clim 23:6624–6640

Dee DP et al (2011) The ERA-interim reanalysis: configuration and performance of the data assimilation system. Q J R Meteorol Soc 137:553–597

Ding Y, He C (2006) The summer monsoon onset over the tropical eastern Indian Ocean: the earliest onset process of the Asian summer monsoon. Adv Atmos Sci 23(6):940–950

Dixit V, Srinivasan J (2011) The role of vertical shear of the meridional winds in the northward propagation of ITCZ. Geophys Res Lett 38:L08812. doi:10.1029/2010GL046601

Drbohlav HKL, Wang B (2005) Mechanism of the northward-propagating intraseasonal oscillation: insights from a zonally symmetric model. J Clim 18:952–972

Fu X, Wang B, Li T, McCreary J (2003) Coupling between northward-propagating, intraseasonal oscillations and sea surface temperature in the Indian Ocean. J Atmos Sci 60(15):1733–1753

Goswami BN (2005) South Asian monsoon. In: Lau WKM, Waliser DE (eds) Intraseasonal variability in the atmosphere–ocean climate system. Springer, Berlin, pp 19–61

Hsu PC, Li T (2012) Role of the boundary layer moisture asymmetry in causing the eastward propagation of the Madden–Julian oscillation. J Clim 25:4914–4931

Jiang X, Li T (2005) Re-initiation of the boreal summer intraseasonal oscillation in the tropical Indian Ocean. J Clim 18:3777–3795

Jiang X, Li T, Wang B (2004) Structures and mechanisms of the northward propagating boreal summer intraseasonal oscillation. J Clim 17:1022–1039

Kang IS, Kim D, Kug JS (2010) Mechanism for northward propagation of boreal summer intraseasonal oscillation: convective momentum transport. Geophys Res Lett 37:L24804. doi:10.1029/2010GL045072

Kemball-Cook S, Wang B (2001) Equatorial waves and air-sea interaction in the boreal summer intraseasonal oscillation. J Clim 14:2923–2942

Lawrence DM, Webster PJ (2002) The boreal summer intraseasonal oscillation: relationship between northward and eastward movement of convection. J Atmos Sci 59:1593–1606

Li T (2010) Monsoon climate variabilities. In: Sun DZ, Frank B (eds) Climate dynamics: why does climate vary? Geophys. Monogr. Ser. doi:10.1029/2008GM000782

Li T, Wang B (1994) The influence of sea surface temperature on tropical intraseasonal oscillation: a numerical study. Mon Weather Rev 122:2349–2362

Li T, Wang B (2005) A review on the western North Pacific monsoon: synoptic-to-interannual variabilities. Terr Atmos Ocean Sci 16:285–314

Li T, Zhou C (2009) Planetary scale selection of the Madden–Julian oscillation. J Atmos Sci 66:2429–2443

Li Z, Yu W, Li T, Murty VSN, Tangang F (2012) Bimodal character of cyclone climatology in Bay of Bengal modulated by monsoon seasonal cycle. J Clim (in revision)

Liebmann B, Smith CA (1996) Description of a complete (interpolated) outgoing longwave radiation dataset. Bull Am Meteorol Soc 77:1275–1277

Madden RA (1986) Seasonal variations of the 40–50 day oscillation in the tropics. J Atmos Sci 43:3138–3158

Madden RA, Julian PR (1971) Detection of a 40–50 day oscillation in the zonal wind in the tropical Pacific. J Atmos Sci 28:702–708

Madden RA, Julian PR (1972) Description of global-scale circulation cells in the tropics with a 40–50 day period. J Atmos Sci 29:3138–3158

Murakami T (1980) Empirical orthogonal function analysis of satellite-observed outgoing longwave radiation during summer. Mon Weather Rev 108:205–222

Salby ML, Hendon HH (1994) Intraseasonal behavior of clouds, temperature, and motion in the tropics. J Atmos Sci 51:2207–2224

Wang B (2006) The Asian monsoon. Springer, Praxis, pp 61–62

Wang B, Li T (1994) Convective interaction with boundary-layer dynamics in the development of a tropical intraseasonal system. J Atmos Sci 51:1386–1400

Wang B, Rui H (1990) Synoptic climatology of transient tropical intraseasonal convection anomalies: 1975–1985. Meteorol Atmos Phys 44:43–61

Wang B, Webster P, Kikuchi K, Yasunari T, Qi Y (2006) Boreal summer quasi-monthly oscillation in the global tropics. Clim Dyn 27:661–675. doi:10.1007/s00382-006-0163-3

Wu MLC, Schubert SD, Suarez MJ, Pegion PJ, Waliser DE (2006) Seasonality and meridional propagation of the MJO. J Clim 19:1901–1921

Yanai M, Esbensen S, Chu JH (1973) Determination of bulk properties of tropical cloud clusters from large-scale heat and moisture budgets. J Atmos Sci 30:611–627

Yasunari T (1979) Cloudiness fluctuations associated with the northern hemisphere summer monsoon. J Meteorol Soc Japan 57:227–242

Zhang C, Dong M (2004) Seasonality in the Madden–Julian oscillation. J Clim 17:3169–3180

Zhang Z, Chan JCL, Ding Y (2004) Characteristics, evolution and mechanisms of the summer monsoon onset over Southeast Asia. Int J Climatol 24:1461–1482. doi:10.1002/joc.1082

Zhu W, Li T, Fu X, Luo JJ (2010) Influence of the maritime continent on the boreal summer intraseasonal oscillation. J Meteorol Soc Japan 88:395–407